Competing Reactions with Initially Separated Components

Haim Taitelbaum,[1] Baruch Vilensky,[1] Anna Lin,[2] Andrew Yen,[2] Yong-Eun Lee Koo,[2,3] and Raoul Kopelman[2]
[1]*Department of Physics, Bar-Ilan University, Ramat-Gan 52900, Israel*
[2]*Department of Chemistry, University of Michigan, Ann Arbor, Michigan 48109-1055*
[3]*Inorganic Division, Department of Chemistry, National Institute of Technology and Quality, 2 Chungand-dong, Kwachon, Kyounggido, Korea*
(Received 13 February 1996)

The first theoretical and experimental study of a competitive reaction with initially separated components is presented. Rich spatiotemporal reaction front patterns are produced by a simple theoretical reaction-diffusion model. Such patterns are observed experimentally for the reaction Cr^{3+} + xylenol orange (XO) → products. The conditions for these front patterns are significant differences in the microscopic reaction constants and in the initial densities of the competing species. [S0031-9007(96)00897-6]

PACS numbers: 82.20.–w, 82.30.–b, 05.40.+j

In a series of recent papers [1–16], it has been shown that elementary reaction-diffusion systems with initially separated components have very unusual dynamical properties. For the elementary reaction $A + B \rightarrow C$, the initial separation of reactants leads to the formation of a dynamic reaction front. The presence of such a reaction interface is characteristic of many processes in nature [17–22]. Interesting properties of the front are the global reaction rate $R(t)$, the location of the center of the reaction front $x_f(t)$, the width of the front $w(t)$, and the local reaction rate at the center of the front $R(x_f, t)$. These reaction rate and front properties have been shown to follow a nonclassical behavior, with anomalous time exponents [1,5,6].

The first level of complexity in chemical reaction kinetics is *competing* elementary reactions, which occur in many chemical systems [23]. These reactions also provide the simplest case for the formation of a complex reaction front pattern. In this Letter we show how such a pattern can be simply accounted for by two competing elementary reactions; two *similar* species, A_1 and A_2, on one side of the initially separated system, compete to react with the species on the other side of the system, B, according to the scheme

$$A_1 + B \xrightarrow{k_1} C_1 , \tag{1a}$$

$$A_2 + B \xrightarrow{k_2} C_2 . \tag{1b}$$

These two processes are taking place simultaneously, each with a different microscopic reaction constant, k_1 and k_2.

In the simplest model of the $A + B \rightarrow C$ initially separated system, the following set of mean-field reaction-diffusion equations for the local concentrations ρ_a, ρ_b has been assumed to describe the system [1]:

$$\frac{\partial \rho_a}{\partial t} = D_a \nabla^2 \rho_a - k \rho_a \rho_b , \tag{2a}$$

$$\frac{\partial \rho_b}{\partial t} = D_b \nabla^2 \rho_b - k \rho_a \rho_b , \tag{2b}$$

where D_a, D_b are the diffusion constants, and k is the microscopic reaction constant. These equations are subject to the initial separation condition along the x axis,

$$\rho_a(x, 0) = a_0[1 - H(x)],$$

$$\rho_b(x, 0) = b_0 H(x) , \tag{2c}$$

where a_0, b_0 are the initial densities and $H(x)$ is the Heaviside step function, so that the A's are initially uniformly distributed on the left side ($x < 0$), and the B's on the right side ($x > 0$) of the initial boundary. In the mean-field description, which is valid [7] above $d = 2$, the local production rate of C, is defined by the term $R(x, t) = k \rho_a(x, t) \rho_b(x, t)$, which is the basis for defining all other quantities of interest [1]. In our model (1), which allows for the existence of more than a single species on one side of the initially separated system, the products C_1 and C_2 are assumed to be either identical or experimentally indistinguishable. Thus the local reaction rate of this system will be of the form

$$R(x, t) = k_1 \rho_{a_1}(x, t) \rho_b(x, t) + k_2 \rho_{a_2}(x, t) \rho_b(x, t) . \tag{3}$$

We have studied this system using a generalized discrete version of the evolution equation (2). At each time unit n all species perform a discrete diffusion step, using the exact enumeration method [24], followed by reaction events according to the scheme (1). Finite probabilities of reaction replace the reaction constants k_1, k_2, in the spirit of [5]. We have assumed equal diffusion coefficients for all species and have studied a wide range of microscopic reaction constants and fractions of the A_i's out of the total A density.

We have found that when k_1 and k_2 differ by several orders of magnitude, and when the faster reacting A_1 species is only a very small fraction of the total A density ($A = A_1 + A_2$), the reaction front splits into two centers, and the global reaction rate is nonmonotonic in time. In the following, we present the results for reaction constants $k_1 = 1$ and $k_2 = 10^{-4}$, and initial densities $a_1 = 3\%$ and $a_2 = 97\%$ of the total A density. Figure 1 shows the

 0031-9007/96/77(8)/1640(4)$10.00

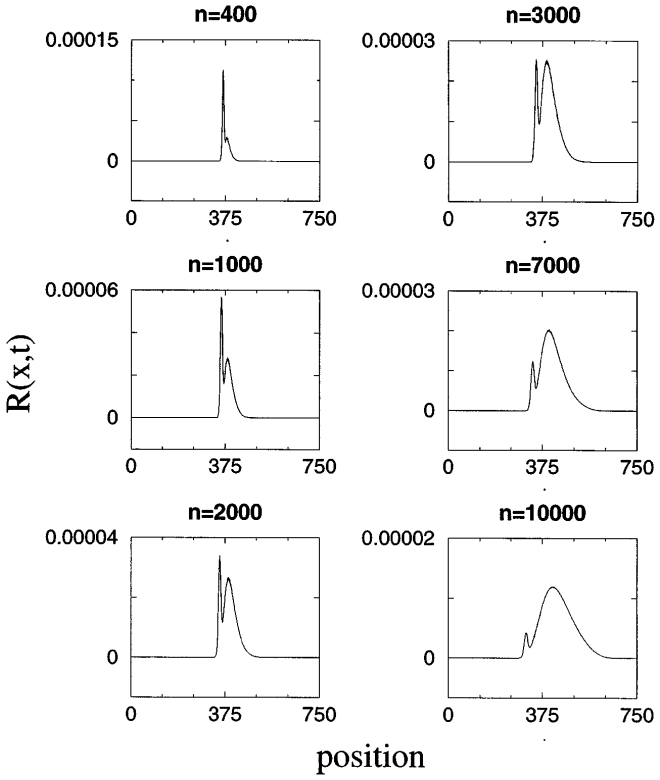

FIG. 1. Numerical results for the time evolution of the spatial profile of the local production rate $R(x,t)$, for $k_1 = 1$, $k_2 = 10^{-4}$, and $a_1 = 3\%$, $a_2 = 97\%$ of the total A density. The front's initial position is at 375.

temporal evolution of the local production rate, $R(x,t)$, as obtained by the superposition of the two processes according to Eq. (3). The A_1 and A_2 species are initially located on the left side of the reaction front, while the B species are initially located on the right. At early time (i.e., $n = 400$), there is already evidence of the existence of two reaction centers. The sharper left peak is a result of the reaction of B with the faster reacting, low density species A_1, while the right peak is a result of the reaction of B with the slower reacting, high density species A_2. As time increases, the contribution of the faster reaction, (1a), decreases, due to the lower A_1 density, and the contribution of the slower reaction, (1b), increases. In the asymptotic time region, the front resulting from the slow reaction becomes dominant, and the left peak disappears.

Figure 2 shows the nonmonotonic behavior of the *global* reaction rate, $R(t) = \int_{-\infty}^{+\infty} R(x,t)dx$, as a function of time. In the simple initially separated system, with only one reaction process, this quantity exhibits a crossover from a $t^{1/2}$ increase to a $t^{-1/2}$ decrease, which occurs at a time proportional to k^{-1} [5]. In the competing reaction system, the global rate of the faster reaction, (1a), the primary early-time contributor to the superposed global reaction rate, begins to decay after time proportional to k_1^{-1}, at which time the global rate of the slower reaction, (1b), becomes the main contributor to the

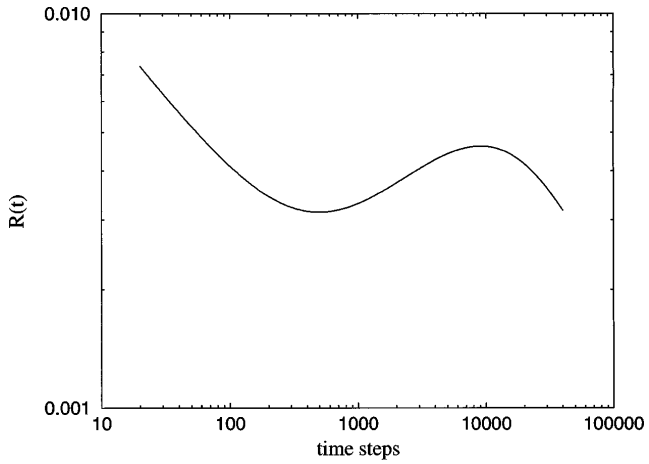

FIG. 2. Numerical results of the global rate $R(t)$ as a function of time for the double-reaction scheme of Eq. (3), for the same parameters as in Fig. 1.

global rate of the competitive system, which gradually increases up to a time proportional to k_2^{-1} when the second crossover occurs. The ratio of the A densities ensures that there is enough material left for the slower process.

In order to test these theoretical predictions experimentally, we use the chemical reaction [25,26] of Cr^{3+} with xylenol orange (XO). We propose that Cr^{3+} is the analog of A and XO is the analog of B in the model. The main subspecies of Cr^{3+} (A_2), which reacts very slowly with XO [6], comes from the aggregation of Cr^{3+} ions in aqueous solution, while the other subspecies, A_1, is the nonaggregated form. The degree of this aggregation is highly dependent on pH. Stünzi *et al.* [27] studied the aggregation of Cr^{3+} occurring in aqueous solution, where the Cr^{3+} ions bind with H_2O, -OH, and other Cr^{3+} ions to form dimers, trimers, and other, higher order aggregate species of Cr^{3+}, (known as oligomers), as well as nonag-

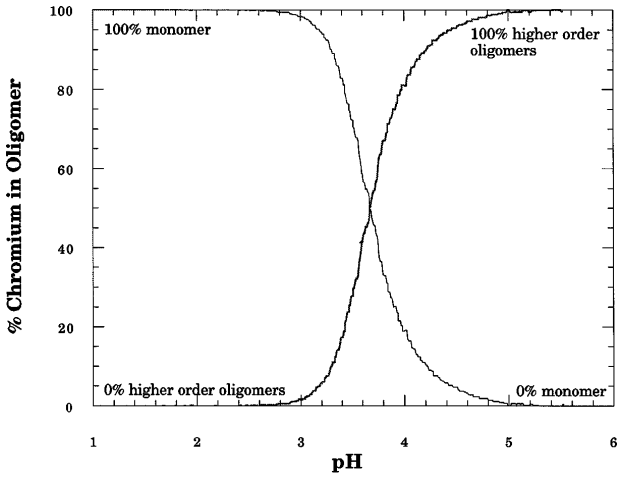

FIG. 3. Percentage of Cr^{3+} monomers and higher order oligomers as a function of the pH of the solution. At pH = 4.5 the chromium consists of 3% monomer and 97% of higher order oligomers. After Stünzi *et al.* [27].

gregated forms (monomers) with only one ion of Cr^{3+}. Figure 3 shows their results for the percentage of aggregated vs nonaggregated Cr^{3+} ions as a function of pH, obtained from a *four year* time study of the evolution and equilibrium of aqueous Cr^{3+} solutions at room temperature. At pH 4.5, which was the pH in our experiments, about 3% of the Cr^{3+} in aqueous solution is in nonaggregated form (monomer), and 97% is in the form of aggregates (oligomers). Thus the monomer is the fast reacting, low density species (A_1), and the higher order oligomers constitute the slow reacting, high density species (A_2). We note that the B species XO has also 10 possible ionic forms (tautomers) as a function of pH of the aqueous solution [28]. However, we disregard XO as a possible source of competing species, since the theoretical model suggests that the two similar species should differ significantly in their reactivity with the other species on the other side of the system, but it is very unlikely that the ionic forms of XO have substantially different rate constants in their reaction with chromium [29,30].

In our experimental system, aqueous gel solutions of Cr^{3+} and XO, adjusted to pH 4.5, are introduced into opposite ends of a long, thin capillary tube (reaction vessel), the Cr^{3+} from the left, and the XO from the right. The initial concentrations are $a_0 = 1.05 \times 10^{-3}$ M for the *total* Cr^{3+} density, and $b_0 = 1.1 \times 10^{-4}$ M for the XO. Adding gelatin to the solutions deters convection, thus aiding in the formation of a sharp reaction boundary where the two solutions meet. It also buffers the solutions, keeping the pH relatively constant over time (a few hours). Product formation with time is measured via optical absorption measurements, using the system described in detail in Ref. [3]. Successive absorbance profiles of the product formation are obtained by periodically scanning along a defined length of the reaction vessel. Light is selectively collected using a 570 $\pm$ 10 nm bandpass filter, and we assume that both products (C_1 and C_2) are detectable at this wavelength. Scans are made every few minutes and each scan takes about 30 s. The time intervals between successive scans increase from 10 min at relatively short times up to 60 min for long times because the total production is much smaller at later times. Subtracting successive absorbance profiles and dividing by the time interval, one obtains the product absorbance per time, which is proportional to the local instantaneous production rate $R(x, t)$.

Figure 4 shows the experimental results for the temporal evolution of the product absorbance per time. Apart from a little difference in the amplitude heights at the longer times, the experimental two-peak pattern mirrors the theoretical results for $R(x, t)$ in Fig. 1. At early times, the primary contribution derives from the faster reacting nonaggregated Cr^{3+} species (A_1), while at later times the main contribution is from the slower reacting Cr^{3+} aggregate species (A_2), which diffuses farther right into the reaction zone before reacting. In Fig. 5 we show the experimental results of the spatially integrated absorbance per time. This quantity exhibits a nonmonotonic time behavior, in excellent accord with the results of the theoretical model for the global rate $R(t)$ (Fig. 2). The initial decay due to the faster process is followed by an increase caused by the slower reaction, which starts to dominate the entire process. Finally, at longer times, the reactant

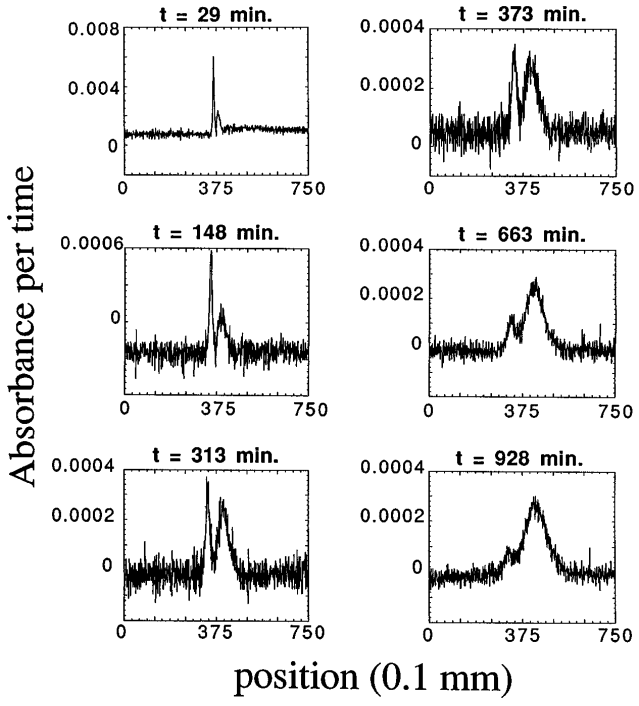

FIG. 4. Experimental profiles of the product absorbance per time at various times. These profiles are proportional to the rate $R(x, t)$ and are in very good agreement with the theoretical predictions presented in Fig. 1. The initial position of the front is at 375, in units of 0.1 mm.

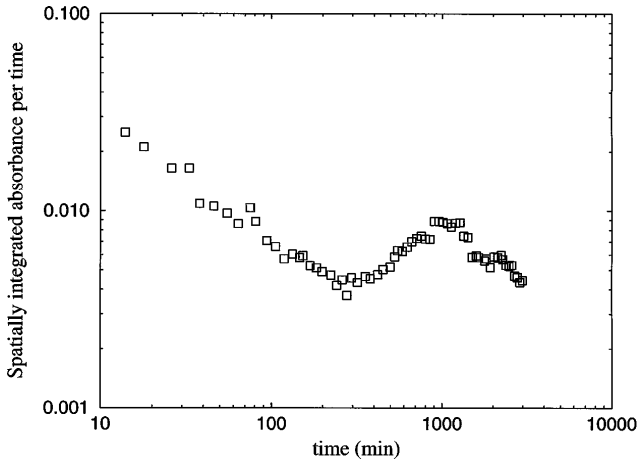

FIG. 5. Experimental results of the spatially integrated absorbance per time, which is proportional to the global reaction rate $R(t)$. The results are in accord with the theoretical results shown in Fig. 2.

concentration of all species is sufficiently low and the global rate decreases asymptotically.

In summary, we have presented a model for a system of two competing reactions where the reactants are initially separated in space. Reaction constants which differ by several orders of magnitude and initial densities of the competing species which are also very different produce novel spatial patterns at the reaction front and a nonmonotonic behavior of the global reaction rate. We observe these spatial and temporal behaviors experimentally using the reaction of Cr^{3+} with XO, where the species that compete for reaction with the XO are Cr^{3+} aggregate and nonaggregate ions in aqueous solution.

We acknowledge support by the Israel Science Foundation (H.T.), the Bi-National (Israel-US) Science Foundation (R.K.), and NSF Grant No. DMR-94-107-09 (R.K.).

[1] L. Gálfi and Z. Rácz, Phys. Rev. A **38**, 3151 (1988).
[2] Y. E. Koo, L. Li, and R. Kopelman, Mol. Cryst. Liq. Cryst. **183**, 187 (1990).
[3] Y-E. L. Koo and R. Kopelman, J. Stat. Phys. **65**, 893 (1991).
[4] Z. Jiang and C. Ebner, Phys. Rev. A **42**, 7483 (1990).
[5] H. Taitelbaum, S. Havlin, J. E. Kiefer, B. Trus, and G. H. Weiss, J. Stat. Phys. **65**, 873 (1991).
[6] H. Taitelbaum, Y-E. L. Koo, S. Havlin, R. Kopelman, and G. H. Weiss, Phys. Rev. A **46**, 2151 (1992).
[7] S. Cornell, M. Droz, and B. Chopard, Phys. Rev. A **44**, 4826 (1991).
[8] M. Araujo, S. Havlin, H. Larralde, and H. E. Stanley, Phys. Rev. Lett. **68**, 1791 (1992).
[9] E. Ben-Naim and S. Redner, J. Phys. A **25**, L575 (1992).
[10] H. Larralde, M. Araujo, S. Havlin, and H. E. Stanley, Phys. Rev. A **46**, 855 (1992); **46**, R6121 (1992).
[11] B. Chopard, M. Droz, T. Karapiperis, and Z. Rácz, Phys. Rev. E **47**, R40 (1993).
[12] S. Cornell and M. Droz, Phys. Rev. Lett. **70**, 3824 (1993); S. Cornell, *ibid.,* **75**, 2250 (1995).
[13] M. Araujo, H. Larralde, S. Havlin, and H. E. Stanley, Phys. Rev. Lett. **71**, 3592 (1993); **75**, 2251 (1995).
[14] B. Vilensky, S. Havlin, H. Taitelbaum, and G. H. Weiss, J. Phys. Chem. **98**, 7325 (1994).
[15] B. P. Lee and J. Cardy, Phys. Rev. E **50**, R3287 (1994).
[16] S. Cornell, Z. Koza, and M. Droz, Phys. Rev. E **52**, 3500 (1995).
[17] R. E. Liesegang, Naturwiss. Wochenschr. **11**, 353 (1896).
[18] H. K. Henisch, *Crystals in Gels and Liesegang Rings* (Cambridge University Press, Cambridge, 1988).
[19] D. Avnir and M. Kagan, Nature (London) **307**, 717 (1984), and references cited therein.
[20] G. T. Dee, Phys. Rev. Lett. **57**, 275 (1986).
[21] B. Heidel, C. M. Knobler, R. Hilfer, and R. Bruinsma, Phys. Rev. Lett. **60**, 2492 (1988).
[22] K.F. Mueller, Science **225**, 1021 (1984).
[23] J. I. Steinfeld, J. Francisco, and W. Hase, *Chemical Kinetics and Dynamics* (Prentice-Hall, Englewood Cliffs, New Jersey, 1989).
[24] S. Havlin and D. Ben-Avraham, Adv. Phys. **36**, 695 (1987).
[25] F. D. Snell, *Photometric and Fluorometric Methods of Analysis* (Wiley, New York, 1978), Part 1.
[26] O. Valci, I. Nemcova, and V. Suk, *Handbook of Triarylmethane and Xanthene Dyes* (CRC Press, Boca Raton, Florida, 1985).
[27] H. Stünzi, L. Spiccia, F. P. Rotzinger, and W. Marty, Inorg. Chem. **28**, 66 (1989).
[28] B. Řehák and J. Körbl, Collection Czechoslov. Chem. Commun. **25**, 797 (1960).
[29] F. J. Welcher, *Analytical Uses of Ethylenediamine Tetraacetic Acid* (D. Van Nostrand Company, Princeton, New Jersey, 1958).
[30] V. Pecoraro (private communication).